

ARTICLE

DOI: 10.1038/s41467-018-07074-4

OPEN

# Unusually complex phase of dense nitrogen at extreme conditions

Robin Turnbull <sup>1</sup>, Michael Hanfland<sup>2</sup>, Jack Binns <sup>3</sup>, Miguel Martinez-Canales<sup>1</sup>, Mungo Frost <sup>1,4</sup>, Miriam Marqués<sup>1</sup>, Ross T. Howie<sup>3</sup> & Eugene Gregoryanz <sup>5</sup>

Nitrogen exhibits an exceptional polymorphism under extreme conditions, making it unique amongst the elemental diatomics and a valuable testing system for experiment-theory comparison. Despite attracting considerable attention, the structures of many high-pressure nitrogen phases still require unambiguous determination. Here, we report the structure of the elusive high-pressure high-temperature polymorph  $\iota$ -N<sub>2</sub> at 56 GPa and ambient temperature, determined by single crystal X-ray diffraction, and investigate its properties using ab initio simulations. We find that  $\iota$ -N<sub>2</sub> is characterised by an extraordinarily large unit cell containing 48 N<sub>2</sub> molecules. Geometry optimisation favours the experimentally determined structure and density functional theory calculations find  $\iota$ -N<sub>2</sub> to have the lowest enthalpy of the molecular nitrogen polymorphs that exist between 30 and 60 GPa. The results demonstrate that very complex structures, similar to those previously only observed in metallic elements, can become energetically favourable in molecular systems at extreme pressures and temperatures.

<sup>1</sup>Centre for Science at Extreme Conditions and School of Physics and Astronomy, University of Edinburgh, Edinburgh, UK. <sup>2</sup>European Synchrotron Radiation Facility, Grenoble, France. <sup>3</sup>Center for High Pressure Science & Technology Advanced Research, Shanghai, China. <sup>4</sup>SLAC National Accelerator Laboratory, Menlo Park, CA, USA. <sup>5</sup>Key Laboratory of Materials Physics, Institute of Solid State Physics, Chinese Academy of Sciences, Hefei, China. Correspondence and requests for materials should be addressed to E.G. (email: [eugene@issp.ac.cn](mailto:eugene@issp.ac.cn))

Extreme-conditions research has uncovered a new regime of complex structures in elemental materials which, counter-intuitively, deviate from simple close packing with the application of pressure. This pressure-induced complexity has previously been exemplified by the structural diversity observed in light alkali and alkaline-earth metals<sup>1–3</sup>. In contrast, such complex, large volume structures have neither been observed, nor have they been predicted, in elemental simple-molecular systems. The nitrogen molecule is used to explore high-pressure phenomena in experimental and theoretical extreme-conditions research because its significant polymorphism makes it unique amongst diatomic elements. Since the first cryogenic experiments of the early 20th century, 15 unique phases of solid nitrogen have been reported over a wide range of pressures and temperatures, including: 12 molecular phases<sup>4–12</sup>, two non-molecular phases<sup>13,14</sup> and an amorphous state<sup>15</sup>, as well as numerous predicted structures<sup>16–20</sup>. The majority of the phases were detected through spectroscopic techniques, which, although useful for providing structural ‘fingerprints’, do not reveal the underlying crystal structures. Consequently, the structures of many of the nitrogen phases remain unknown despite experimental efforts, due primarily to challenges associated with producing and analysing single-crystal samples in the geometrically constrained environment of diamond anvil cells (DACs).

The pressure-temperature ( $P$ - $T$ ) phase and reaction diagram of nitrogen (illustrated in Fig. 1a) has been a focal point in high-pressure research for the past 15 years since the discovery of the high-temperature high-pressure phases<sup>12</sup> known as  $\iota$ -N<sub>2</sub> and  $\theta$ -N<sub>2</sub>. The phase which nitrogen adopts strongly depends on the  $P$ - $T$  history of the system, and both the  $\iota$ -N<sub>2</sub> and  $\theta$ -N<sub>2</sub> phases are recoverable to ambient temperature and much lower pressures than those required for their synthesis<sup>12</sup> (shown in Fig. 1a). The structures  $\iota$ -N<sub>2</sub> and  $\theta$ -N<sub>2</sub> have remained unknown since their discovery. The  $\iota$ -N<sub>2</sub> phase has proved particularly elusive, with only the original synthesis study providing experimental data<sup>12</sup> which was limited to Raman and infra-red spectroscopy. Subsequently, one work claimed the production of  $\iota$ -N<sub>2</sub> after temperature-quenching fluid-N<sub>2</sub> at high-pressure but provided no supporting evidence<sup>21</sup>. Other studies have been unable to observe  $\iota$ -N<sub>2</sub> despite replicating the correct  $P$ - $T$  conditions<sup>22</sup>,

instead reporting recrystallization of fluid-N<sub>2</sub> into the conventional  $\delta$ -N<sub>2</sub> and  $\epsilon$ -N<sub>2</sub><sup>23</sup>, thereby casting ambiguity over the  $P$ - $T$  path and conditions at which  $\iota$ -N<sub>2</sub> can be synthesised.

## Results

**$\iota$ -N<sub>2</sub> synthesis and Raman spectra.** In this study we have unequivocally synthesised a single crystal of  $\iota$ -N<sub>2</sub> in a resistively heated DAC from  $\epsilon$ -N<sub>2</sub> at 65 GPa and 750 K. (See Methods section for further details). The  $\epsilon$ -N<sub>2</sub>  $\rightarrow$   $\iota$ -N<sub>2</sub> transition was initially identified by Raman spectroscopy and visual observation, as shown in Fig. 1b–e. The transition is characterised by the loss of the  $\epsilon$ -N<sub>2</sub>  $\nu_1$  vibrational mode, as shown in the Raman spectra across the synthesis  $P$ - $T$  path in Supplementary Figure 1. A video of the phase transition can be seen in Supplementary Movie 1. Typically,  $\epsilon$ -N<sub>2</sub> has a birefringent appearance which became uniformly smooth on entering the  $\iota$ -N<sub>2</sub> phase. Phase boundaries between  $\epsilon$ -N<sub>2</sub> and  $\iota$ -N<sub>2</sub> were clearly observed moving across the sample chamber (also indicated by arrows in Fig. 1c) and the transition progressed to completion over several minutes, indicating a kinetically slow phase transition which requires the sustained elevated temperatures generated by resistive heating techniques. This observation may explain why previous studies, which utilised laser heating, have struggled to produce the  $\iota$ -N<sub>2</sub> phase at the same  $P$ - $T$  conditions as the technique suffers from transient and localised peak-temperatures within the sample<sup>24</sup>. Additionally, Raman spectra of the  $\iota$ -N<sub>2</sub>  $\rightarrow$   $\epsilon$ -N<sub>2</sub> back-transformation on isothermal decompression at ambient temperature (Supplementary Figure 2) show the re-emergence of the  $\epsilon$ -N<sub>2</sub>  $\nu_1$  vibrational mode between 20–25 GPa, in agreement with ref.<sup>12</sup>.

After recovery to ambient temperature, high resolution Raman spectra were acquired to confirm the synthesis of  $\iota$ -N<sub>2</sub> (Fig. 1e). In total eight vibrational modes were resolved, all of which originate from molecular N<sub>2</sub> centres. The lowest frequency vibrational mode,  $\nu_1$  (2409 cm<sup>-1</sup> at 56 GPa), is the most intense by approximately an order of magnitude. The additional higher frequency vibrational modes ( $\nu_2$ – $\nu_8$ ) are all within 30 cm<sup>-1</sup> of  $\nu_1$ , describing an unusually complex vibrational spectrum for an elemental molecular system. The lattice modes of  $\iota$ -N<sub>2</sub>, shown in Supplementary Figure 3, appear sharp and well-defined indicating

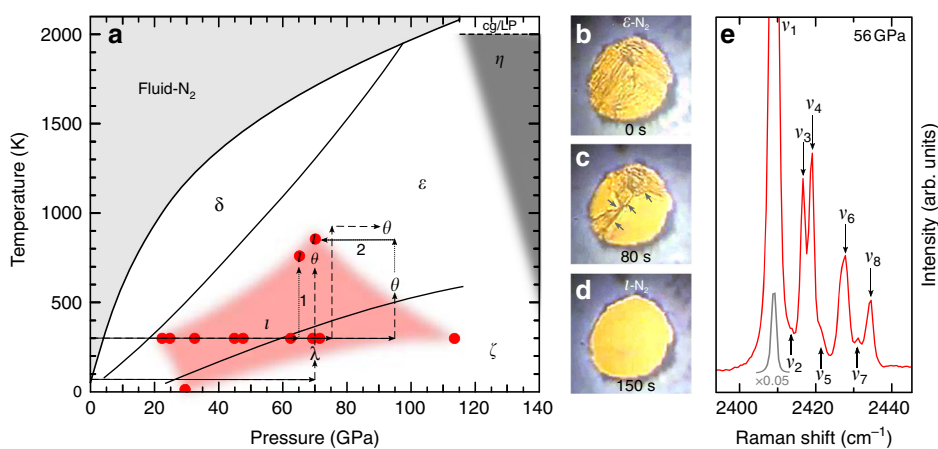


**Fig. 1** The nitrogen phase and reaction diagram. **a** The reported  $P$ - $T$  paths to the high-temperature molecular phases  $\iota$ -N<sub>2</sub> and  $\theta$ -N<sub>2</sub> are shown with dotted and dashed arrows respectively. The red shaded region approximates the known stability field of  $\iota$ -N<sub>2</sub> based on a combination of our Raman measurements and those of ref.<sup>12</sup>. Path 1: Isobaric heating of  $\epsilon$ -N<sub>2</sub> to 750 K at 65 GPa, as performed in this study. Path 2: Isothermal decompression of  $\theta$ -N<sub>2</sub> to 69 GPa at 850 K.  $P$ - $T$  paths and data points are taken from refs.<sup>11,12,21,22</sup> which identify the phases through Raman spectroscopy. Black phase-boundaries are based on refs.<sup>21–23</sup>. Phases  $\alpha$ ,  $\beta$ ,  $\gamma$ ,  $\delta^*$ ,  $\zeta$ ,  $\kappa$  and  $\lambda$ -N<sub>2</sub> are omitted for clarity. **b–d** Micrographs of the visual changes across the  $\epsilon$ -N<sub>2</sub>  $\rightarrow$   $\iota$ -N<sub>2</sub> phase transition. The sample is approximately 60  $\mu$ m in diameter and 15  $\mu$ m thick. The time from the onset of the phase-transition is shown on each frame. The arrows in **c** indicate the progression of the  $\epsilon$ -N<sub>2</sub>  $\rightarrow$   $\iota$ -N<sub>2</sub> phase boundary. **e** Vibrational Raman spectrum of  $\iota$ -N<sub>2</sub> once recovered to ambient temperature. The inset spectrum (light grey) shows  $\nu_1$  scaled by a factor of 0.05 to display it fully



pressure region of interest. However none of the proposed structures of ref.<sup>18</sup> have been observed experimentally. (Note that although the ' $P2_1/c$ -candidate' of ref.<sup>18</sup> shares its space group with  $t$ -N<sub>2</sub>, it contains only two molecules). The calculated  $t$ -N<sub>2</sub> volume

per atom shows a volume decrease of approximately 2.5% compared to  $\epsilon$ -N<sub>2</sub> at ambient temperature and 56 GPa (Fig. 4b) which is consistent with a spontaneous high-pressure phase transition such as the one observed here.

The calculated Raman spectrum of  $t$ -N<sub>2</sub> (Supplementary Figure 4) reproduces the high frequency vibrational structure, with eight active modes, of which the lowest frequency mode is at least an order of magnitude more intense than the others. The calculated intensities of the low frequency modes (Supplementary Figure 5) are two orders of magnitude lower than those of the most intense vibron, in close agreement with experiment. Additionally, ab initio random structure searches (AIRSS) were performed using all available experimental  $t$ -N<sub>2</sub> constraints, such as the lattice parameters, space group (subgroups were allowed), and number of molecules per cell. The details of the searches can be found in the Methods section below. The experimentally observed  $t$ -N<sub>2</sub> structure was yielded twice, and, of >3100 structures generated, none had a lower enthalpy than  $t$ -N<sub>2</sub>, with the next best being a purely molecular structure at 26 meV/molecule greater than  $t$ -N<sub>2</sub>. Such large systems are not typically attempted with contemporary AIRSS techniques due to computational constraints, and it is certainly noteworthy that  $t$ -N<sub>2</sub> was found despite the large unit cell and weak intermolecular interactions. Unconstrained and partially constrained searches favour polymerization at these pressures, resulting in mixed molecular/non-molecular phases similar to those predicted previously<sup>20,27</sup>. It is therefore extremely unlikely that the  $t$ -N<sub>2</sub> structure would have been found without the experimental constraints, thus highlighting the importance of close collaboration between theory and experiment in the search for high-pressure structures.

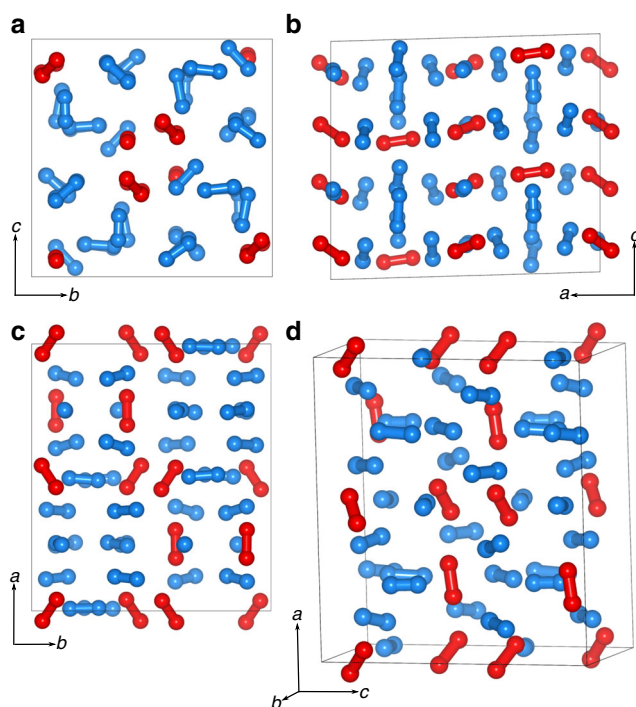


**Fig. 3** The refined crystal structure of  $t$ -N<sub>2</sub>. **a–c** Projections along the  $a$ ,  $b$  and  $c$  axes respectively. **d** A perspective projection of the unit cell. Layered N<sub>2</sub> molecules are shown in blue and oriented molecules are shown in red. Supplementary crystallographic data for the  $t$ -N<sub>2</sub> structure can be obtained free of charge from The Cambridge Crystallographic Data Centre, under deposition number CCDC 1869044

## Discussion

Our study demonstrates that the appearance of complex structures under pressure is not limited only to metallic elements<sup>1–3</sup> and raises the intriguing question of whether unusual phases could be expected in other molecular systems at extreme conditions. The pressure-induced complexity in many metallic elements has been attributed to  $s$ - $p$  or  $s$ - $d$  electronic transfer<sup>28,29</sup> which is clearly not an applicable stability mechanism in the case

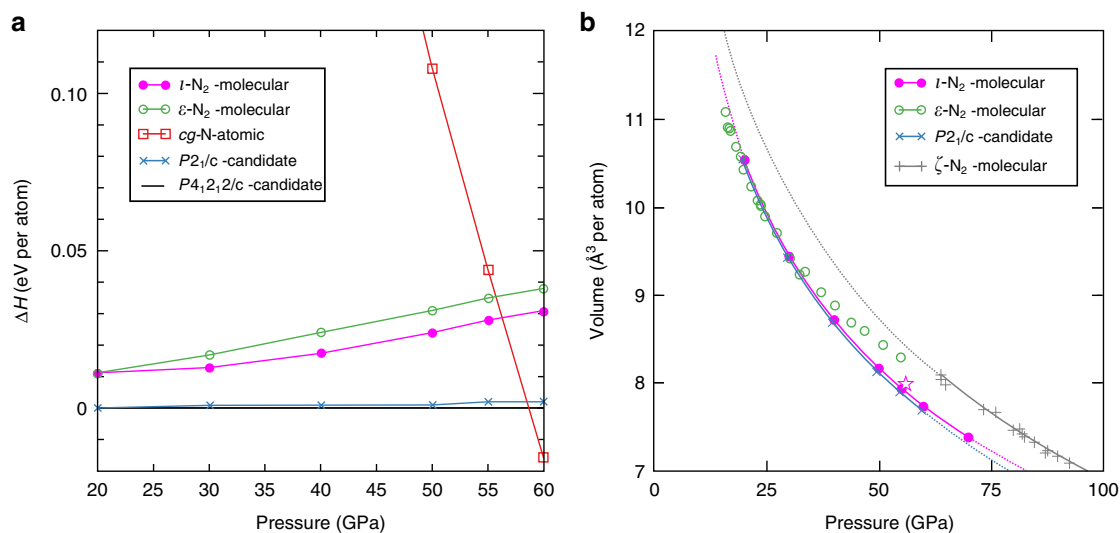


**Fig. 4** The calculated enthalpy and volume per atom for the  $t$ -N<sub>2</sub> structure. **a** Calculated PBE enthalpy differences with respect to the  $P4_12_12$ -candidate structure of ref.<sup>18</sup>. The computed enthalpy of  $t$ -N<sub>2</sub> is more favourable than  $\epsilon$ -N<sub>2</sub> above 20 GPa. Polymeric  $cg$ -N becomes favourable at 58 GPa, in agreement with previous DFT estimates. **b** Calculated volume per atom of  $t$ -N<sub>2</sub> and the  $P2_1/c$ -candidate structure of ref.<sup>18</sup> plotted with experimental data for  $\epsilon$ -N<sub>2</sub> and  $\zeta$ -N<sub>2</sub>. The  $t$ -N<sub>2</sub> volumes are -1% larger than the  $P2_1/c$ -candidate of ref.<sup>18</sup>. The star shows the experimentally determined  $t$ -N<sub>2</sub> volume per atom at 56 GPa and ambient temperature. The experimental data for  $\epsilon$ -N<sub>2</sub> and  $\zeta$ -N<sub>2</sub> are reproduced from ref.<sup>9</sup> and references therein

of the molecular and insulating  $\iota$ -N<sub>2</sub> phase. Therefore, there must be other mechanisms in highly condensed nitrogen which make these very complex configurations favourable. In the ‘disorder-order’ transition from  $\delta$ -N<sub>2</sub> to  $\varepsilon$ -N<sub>2</sub>, the N<sub>2</sub> molecules forego the entropy of their rotational disorder, in favour of occupying less volume, by ordering in certain molecular orientations<sup>10</sup>. In the transition from  $\varepsilon$ -N<sub>2</sub> to  $\iota$ -N<sub>2</sub> however, both phases are characterised by rotationally ordered N<sub>2</sub> molecules. So, what drives the ‘order-order’ transition? In this case the transition is thermodynamically favourable because the volume per atom in the unit cell decreases (as seen in Fig. 4b), whilst the configurational entropy increases due to the larger number of molecules in the unit cell. The  $\varepsilon$ -N<sub>2</sub> to  $\iota$ -N<sub>2</sub> transition is additionally characterised by a rearrangement of the N<sub>2</sub> molecules into layers (as seen in Fig. 3) which may facilitate vibrational resonance coupling, particularly because molecules between layers take a mutually perpendicular orientation<sup>30</sup>, which could play an important role in kinetic favourability. Our DFT calculations find  $\iota$ -N<sub>2</sub> to have the lowest enthalpy of the molecular nitrogen polymorphs for which the structures are known between 30 and 60 GPa, which will have implications for the nitrogen phase diagram. Although some pioneering structural searches on nitrogen<sup>31</sup> have been later confirmed by experiment<sup>13</sup>, these structures were elegantly simple and identified by comparison of powder XRD data with calculated patterns. Our study of  $\iota$ -N<sub>2</sub> shows that in systems with unforeseen complexity, interesting structures could be potentially overlooked without the direction offered by experiment, and that at extreme conditions unusually complex structures may be more energetically favourable in molecular systems. We hope that our results will prompt further investigations into why such complex structures should appear at high pressures in elemental diatomic solids.

## Methods

**Sample preparation.** Research-grade nitrogen (>99.9995% purity, obtained from BOC) was condensed at 77 K and loaded into symmetric DACs equipped with built-in graphite resistive-heaters. Wide opening seats with Boehler-Almax diamonds were used to allow for maximal scattering angle in XRD experiments. Culet sizes were 200  $\mu$ m and rhenium gaskets were pre-indented to 20  $\mu$ m prior to loading. Raman spectroscopy was conducted using the 514 nm emission line of an Ar<sup>+</sup> ion laser. Pressure was controlled via a gas-membrane and pressure was determined using the diamond edge scale<sup>32</sup>. The samples were recovered to ambient-temperature and transported by applying the load of the gas-membrane onto the DAC screws.

**XRD and structural refinement procedure.** Single-crystal XRD data used for refinement were collected at the ID15B beamline at ESRF (Grenoble, France) using a monochromatic beam  $\lambda = 0.411$  Å focused to a spot size of  $10 \times 10$   $\mu$ m. Data were recorded on a MAR555 flat panel detector. The sample was rotated at  $\omega$  over a range of 60° in 0.5° increments. The image-plate shown in Fig. 2 was acquired at the Extreme Conditions Beamline (P02.2) at PETRA III (Hamburg, Germany) using a monochromatic beam  $\lambda = 0.2889$  Å focused to a spot size of  $4 \times 4$   $\mu$ m. Data were recorded on a PerkinElmer XRD 1621 detector. Data were indexed and integrated with CrysAlisPro<sup>33</sup>. A total of 1276 reflections were indexed to a monoclinic lattice with unit-cell dimensions  $a = 9.899(2)$ ,  $b = 8.863(2)$ ,  $c = 8.726(2)$  Å,  $\beta = 91.64(3)^\circ$ ,  $V = 765.2(3)$  Å<sup>3</sup> at 56 GPa. Systematic absence analysis clearly indicated space group  $P2_1/c$ . Data were integrated to a resolution of 0.6 Å with a merged  $R_{\text{int}} = 0.0342$  for 641 unique reflections, a completeness of 18%. The crystal was oriented with the  $c^*$  axis approximately perpendicular to the diamond culets resulting in a very low data coverage along  $c^*$  ( $-15 \leq h \leq 15$ ,  $-14 \leq k \leq 13$ ,  $-5 \leq l \leq 4$ ). The structure was solved by dual-space methods using SHELXT and refinement of the crystal structure was carried out against  $|F^2|$  with the SHELXL refinement package<sup>34,35</sup>. Refinement was limited to an isotropic treatment for all nitrogen atoms, an anisotropic treatment led to refinement instabilities. Rigid bond restraints were applied to all molecular bonds with default estimated standard deviations of 0.004 Å<sup>2</sup>. Intramolecular bond distance restraints do not improve the fit to the data.

**DFT calculations.** DFT calculations of energetics and vibrational spectra were performed with CASTEP<sup>36</sup> 18.1. Energetics were computed using the default CASTEP 18 ultrasoft pseudopotential, a 700 eV energy cutoff and a k-point grid spacing better than 0.04 Å<sup>-1</sup>. In order to estimate the effect of neglected non-local

van der Waals interactions, enthalpies were recalculated including Tkatchenko-Scheffler corrections<sup>37</sup>. The effect is negligible, other than lowering the pressure of the transition to the polymeric *cubic gauche* (*cg*-N) phase. Raman spectra were computed using the DFPT + Finite differences method, using the default CASTEP 18 NC pseudopotentials with a 1250 eV energy cutoff, and a similarly dense k-point grid.

**Structure searches.** Ab initio evolutionary structural searches for the  $\iota$ -N<sub>2</sub> structure were performed with the USPEX<sup>38</sup> code and VASP<sup>39,40</sup>. The initial search space with 1000 structures consisted of atoms and N<sub>2</sub> molecular units. The experimentally proposed  $P2_1/c$  symmetry was imposed on some of the searches, but subgroups of lower symmetry such as  $P1$ ,  $Pc$  and  $P2_1$  were also considered. Initial searches with 104 atoms in the unit cell lead to structures  $\approx 0.052$  eV/atom higher in enthalpy than those with 96 atoms.

A random structure search was performed with AIRSS<sup>41</sup> and CASTEP 18.1, on the experimental cell with 96 atoms. In total, >3100 structures were produced. The most favourable searches were those done enforcing initial N<sub>2</sub> molecules and symmetry, generating structures belonging to the  $P2_1/c$  space group, as well as its subgroups  $P2_1$  and  $Pc$ . We were able to reproduce the experimentally refined cell twice, and this was the lowest enthalpy structure found under these considerations.

## Data availability

Supplementary crystallographic data for the  $\iota$ -N<sub>2</sub> structure can be obtained free of charge from The Cambridge Crystallographic Data Centre, under deposition number CCDC 1869044, via [www.ccdc.cam.ac.uk/structures](http://www.ccdc.cam.ac.uk/structures). The relevant  $\iota$ -N<sub>2</sub> DFT enthalpies, computed Raman spectra and AIRSS calculation data are accessible from the Edinburgh DataShare repository via <https://doi.org/10.7488/ds/2449>. All relevant data are available from the corresponding author upon reasonable request.

Received: 23 May 2018 Accepted: 8 October 2018

Published online: 09 November 2018

## References

- Guillaume, C. L. et al. Cold melting and solid structures of dense lithium. *Nat. Phys.* **7**, 211 (2011).
- Gregoryanz, E. et al. Structural diversity of sodium. *Science* **320**, 1054–1057 (2008).
- Loa, I., Nelmes, R. J., Lundegaard, L. F. & McMahon, M. I. Extraordinarily complex crystal structure with mesoscopic patterning in barium at high pressure. *Nat. Mater.* **11**, 627–632 (2012).
- Donohue, J. A. refinement of the positional parameter in  $\alpha$ -nitrogen. *Acta Crystallogr.* **14**, 1000–1001 (1961).
- Schuch, A. F. & Mills, R. L. Crystal Structures of the three modifications of nitrogen 14 and nitrogen 15 at high pressure. *J. Chem. Phys.* **52**, 6000 (1970).
- Mills, R. L., Olinger, B. & Cromer, D. T. Structures and phase diagrams of N<sub>2</sub> and CO to 13 GPa by X-ray diffraction. *J. Chem. Phys.* **84**, 2837 (1986).
- Hanfland, M., Lorenzen, M., Wassilew-Reul, C. & Zontone, F. Structures of molecular nitrogen at high pressures. *Rev. High. Press. Sci. Technol.* **7**, 787–789 (1998).
- Gregoryanz, E., Goncharov, A. F., Hemley, R. J. & Mao, H.-k. High-pressure amorphous nitrogen. *Phys. Rev. B* **64**, 052103 (2001).
- Gregoryanz, E. et al. High P-T transformations of nitrogen to 170 GPa. *J. Chem. Phys.* **126**, 184505 (2007).
- Stinton, G. W., Loa, I., Lundegaard, L. F. & McMahon, M. I. The crystal structures of  $\delta$  and  $\delta^*$  nitrogen. *J. Chem. Phys.* **131**, 104511 (2009).
- Frost, M., Howie, R. T., Dalladay-Simpson, P., Goncharov, A. F. & Gregoryanz, E. Novel high-pressure nitrogen phase formed by compression at low temperature. *Phys. Rev. B* **93**, 024113 (2016).
- Gregoryanz, E. et al. Raman, infrared, and x-ray evidence for new phases of nitrogen at high pressures and temperatures. *Phys. Rev. B* **66**, 224108 (2002).
- Eremets, M. I., Gavriluk, A. G., Trojan, I. A., Dzivenko, D. A. & Boehler, R. Single-bonded cubic form of nitrogen. *Nat. Mater.* **3**, 558–563 (2004).
- Tomasino, D., Kim, M., Smith, J. & Yoo, C.-s. Pressure-induced symmetry-lowering transition in dense nitrogen to layered polymeric nitrogen (LP-N) with colossal Raman intensity. *Phys. Rev. Lett.* **113**, 1–5 (2014).
- Goncharov, A. F., Gregoryanz, E., Mao, H.-k., Liu, Z. & Hemley, R. J. Optical evidence for a non-molecular phase of nitrogen above 150 GPa. *Phys. Rev. Lett.* **85**, 1262–1265 (2000).
- Li, Y. et al. Route to high-energy density polymeric nitrogen t-N via He-N compounds. *Nat. Commun.* **9**, 722 (2018).
- Wang, X. et al. Cagelike diamondoid nitrogen at high pressures. *Phys. Rev. Lett.* **109**, 175502 (2012).

18. Pickard, C. J. & Needs, R. J. High-pressure phases of nitrogen. *Phys. Rev. Lett.* **102**, 125702 (2009).
19. Ma, Y., Oganov, A. R., Li, Z., Xie, Y. & Kotakoski, J. Novel high pressure structures of polymeric nitrogen. *Phys. Rev. Lett.* **102**, 065501 (2009).
20. Mattson, W. D., Sanchez-Portal, D., Chiesa, S. & Martin, R. M. Prediction of new phases of nitrogen at high pressure from first-principles simulations. *Phys. Rev. Lett.* **93**, 125501 (2004).
21. Goncharov, A. F., Crowhurst, J. C., Struzhkin, V. V. & Hemley, R. J. Triple point on the melting curve and polymorphism of nitrogen at high pressure. *Phys. Rev. Lett.* **101**, 1–4 (2008).
22. Tomasino, D., Jenei, Z., Evans, W. & Yoo, C.-s Melting and phase transitions of nitrogen under high pressures and temperatures. *J. Chem. Phys.* **140**, 244510 (2014).
23. Weck, G. et al. Melting curve and liquid structure of nitrogen probed by x-ray diffraction to 120 GPa. *Phys. Rev. Lett.* **119**, 1–5 (2017).
24. Campbell, A. J. Measurement of temperature distributions across laser heated samples by multispectral imaging radiometry. *Rev. Sci. Instrum.* **79**, 015108 (2008).
25. Katzke, H. & Tolédano, P. Theoretical description of pressure and temperature-induced structural phase transition mechanisms of nitrogen. *Phys. Rev. B* **78**, 064103 (2008).
26. Perdew, J. P., Burke, K. & Ernzerhof, M. Generalized gradient approximations made simple. *Phys. Rev. Lett.* **77**, 3865 (1996).
27. Hirshberg, B., Gerber, R. B. & Krylov, A. I. Calculations predict a stable molecular crystal of N<sub>8</sub>. *Nat. Chem.* **6**, 52 (2014).
28. Skriver, H. L. Crystal structure from one-electron theory. *Phys. Rev. B* **31**, 1909–1923 (1985).
29. Errandonea, D., Boehler, R. & Ross, M. Melting of the alkaline-earth metals to 80 GPa. *Phys. Rev. B* **65**, 1–4 (2002).
30. Scheerboom, M. I. M. & Schouten, J. A. Orientational behavior of solid nitrogen at high pressures investigated by vibrational Raman spectroscopy. *J. Chem. Phys.* **105**, 2553–2560 (1996).
31. Mailhiet, C., Yang, L. H. & McMahan, A. K. Polymeric nitrogen. *Phys. Rev. B* **46**, 14419–14435 (1992).
32. Akahama, Y. & Kawamura, H. Pressure calibration of diamond anvil Raman gauge to 410 GPa. *J. Phys. Conf. Ser.* **215**, 012195 (2010).
33. CrysAlispro (red) version 1.171. 38.41 (2010).
34. Sheldrick, G. M. SHELXT - Integrated space-group and crystal-structure determination. *Acta Crystallogr. A* **71**, 3–8 (2014).
35. Sheldrick, G. M. Crystal structure refinement with SHELXL. *Acta Crystallogr. C: Struct. Chem.* **71**, 3–8 (2015).
36. Clark, S. J. et al. First principles methods using CASTEP. *Z. Krist.* **220**, 567–570 (2005).
37. Tkatchenko, A. & Scheffler, M. Accurate molecular van der Waals interactions from ground-state electron density and free-atom reference data. *Phys. Rev. Lett.* **102**, 073005 (2009).
38. Oganov, A. R. & Glass, C. W. Crystal structure prediction using *ab initio* evolutionary techniques: Principles and applications. *J. Chem. Phys.* **124**, 244704 (2006).
39. Kresse, G. & Furthmüller, J. Efficient iterative schemes for *ab initio* total-energy calculations using a plane-wave basis set. *Phys. Rev. B* **54**, 211169 (1996).
40. Kresse, G. & Joubert, D. From ultrasoft pseudopotentials to the projector augmented-wave method. *Phys. Rev. B* **59**, 1758 (1999).
41. Pickard, C. J. & Needs, R. J. *Ab initio* random structure searching. *J. Phys. Condens. Matter* **23**, 053201 (2011).

## Acknowledgements

R.T. acknowledges studentship funding from EPSRC Grants No. EP/L504956/1 and No. EP/M506515/1. M.F. acknowledges DOE FES funding number FWP100182. M.M. acknowledges support from the ERC grant Hecate. M.M.C. and M.M. are grateful for computational support from the UK national high performance computing service, ARCHER, and the UK Materials and Molecular Modelling Hub, which is partially funded by EPSRC (EP/P020194), for which access was obtained via the UKCP consortium and funded by EPSRC grant ref EP/P022561/1. We acknowledge the European Synchrotron Radiation Facility for provision of synchrotron radiation facilities at the ID15B beamline. Parts of this research were carried out at the light source PETRA III at DESY, a member of the Helmholtz Association (HGF), under proposal I-20160268 EC. We would like to thank Konstantin Glazyrin for assistance in using the Extreme Conditions Beamline (P02.2).

## Author contributions

R.T., M.F. and E.G. conceived and designed the project. R.T., M.H., J.B., M.F. and R.T.H. conducted the experiments. R.T., M.H., J.B., M.F., M.M.C. and E.G. analysed the data. R. T., J.B., M.M.C., M.F., R.T.H. and E.G. wrote the paper. M.M.C. and M.M. performed the DFT calculations.

## Additional information

**Supplementary Information** accompanies this paper at <https://doi.org/10.1038/s41467-018-07074-4>.

**Competing interests:** The authors declare no competing interests.

**Reprints and permission** information is available online at <http://npg.nature.com/reprintsandpermissions/>

**Publisher's note:** Springer Nature remains neutral with regard to jurisdictional claims in published maps and institutional affiliations.



**Open Access** This article is licensed under a Creative Commons Attribution 4.0 International License, which permits use, sharing, adaptation, distribution and reproduction in any medium or format, as long as you give appropriate credit to the original author(s) and the source, provide a link to the Creative Commons license, and indicate if changes were made. The images or other third party material in this article are included in the article's Creative Commons license, unless indicated otherwise in a credit line to the material. If material is not included in the article's Creative Commons license and your intended use is not permitted by statutory regulation or exceeds the permitted use, you will need to obtain permission directly from the copyright holder. To view a copy of this license, visit <http://creativecommons.org/licenses/by/4.0/>.

© The Author(s) 2018